Available online at www.sciencedirect.com
ScienceDirect
Comput. Methods Appl. Mech. Engrg. 345 (2019) 283–301
Computer methods in applied mechanics and engineering
www.elsevier.com/locate/cma

Random field simulation over curved surfaces: Applications to computational structural mechanics

Carl Scarth[a,*,1], Sondipon Adhikari[a], Pedro Higino Cabral[b], Gustavo H.C. Silva[b], Alex Pereira do Prado[b]

[a] *College of Engineering, Swansea University, Bay Campus, Fabian Way, Crymlyn Burrows, Skewen, Swansea, SA1 8EN, United Kingdom*
[b] *Embraer S.A., Av. Brigadeiro Faria Lima, 2170, 12227-901 São José dos Campos, São Paulo, Brazil*

Received 9 March 2018; received in revised form 11 September 2018; accepted 18 October 2018
Available online 2 November 2018

Abstract

It is important to account for inherent variability in the material properties in the design and analysis of engineering structures. These properties are typically not homogeneous, but vary across the spatial coordinates within a structure, as well as from specimen to specimen. This form of uncertainty is commonly modelled using random fields within the Stochastic Finite Element Method. Simulation within this framework can be complicated by the dependence of a random field's correlation function upon the geometry of the domain over which it is defined. In this paper, a new method is proposed for simulating random fields over a general two-dimension curved surface, represented as a finite element mesh. The covariance function is parametrised using the geodesic distance, evaluated using the solution to the 'discrete geodesic problem,' and a point discretisation approach is subsequently applied in order to sample the random field at the nodes of the model. The major contribution of the present work is the development of a methodology for simulating random fields over curved surfaces of arbitrary geometry, with a focus upon non-intrusive application to industrial finite element models using 'off the shelf' commercial software. In order to demonstrate the potential impact of the proposed approach, the algorithm is applied in an uncertainty quantification case study concerning vibration and buckling of an industrial composite aircraft wing model.

Keywords: Stochastic finite element; Random field; Monte Carlo simulation; Uncertainty quantification; Aircraft wing

1. Introduction

The design of engineering structures is a complex and multidisciplinary problem in which efficient designs are sought, while ensuring that undesirable phenomena such as material failure do not occur under the loads encountered by the structure. In practice, all properties and processes are subject to uncertainty, and it is impossible

* Corresponding author.
E-mail addresses: c.scarth@bath.ac.uk (C. Scarth), s.adhikari@swansea.ac.uk (S. Adhikari).
[1] Present Address: Department of Mechanical Engineering, University of Bath, Claverton Down, Bath, BA2 7AY.

https://doi.org/10.1016/j.cma.2018.10.026
0045-7825/

to guarantee precise values for the parameters which govern such behaviour. Furthermore, material properties are not homogeneous, but can vary across different spatial coordinates within a structure. Spatially-varying uncertainty such as this may be modelled within the framework of the Stochastic Finite Element Method [1–3], in which uncertain properties are defined as random fields, and are propagated through structural models discretised by a finite element mesh. Simulating random fields within this framework is complicated by the definition of the correlation function of the random field, which is dependent upon the geometry of the spatial domain over which it is defined. This dependence will be the focus of the present work.

A wide range of approaches may be used to characterise random fields [2,3]. In point discretisation methods, the random field is sampled at discrete locations in the spatial domain. For example, random fields may be evaluated at finite element midpoints [4], or alternatively at the Gauss integration points in order to directly integrate the variability into element stiffness and mass matrices [5]. Random fields may also be interpolated within each element based upon values at discrete locations. For example, polynomial shape functions are used to interpolate nodal field values in the shape function method [6], whereas Optimal Linear Expansion [7] makes use of a Kriging interpolation approach. Rather than sampling point-wise field values, it is also possible to use average values taken across each element [8]. Additionally, it is common to approximate random fields as a series expansion of spatially-dependent deterministic functions multiplied by random coefficients. Orthogonal Series Expansion [9] uses a random sum of orthogonal polynomials, whereas Karhunen–Loève Expansion [1] (KLE) instead approximates the field using eigenvalues and eigenfunctions of the covariance function. These eigenvalues and eigenfunctions used in KLE must be obtained through solution of the Fredholm integral eigenvalue problem. Closed-form solutions exist for some covariance functions defined over simple geometries [1]. In other cases, a variety of methods exist for numerical solution of the Fredholm integral [10], including the Nyström method in which the eigenvalue problem is discretised using numerical integration, and the Galerkin and collocation methods in which eigenfunctions are approximated using basis functions and the resulting residuals are minimised. Also of note, is the spectral representation method [11,12], in which cosine series formulae are used to target correlation structures prescribed as Spectral Density Functions, and sample realisations are generated using the Fast Fourier Transform technique.

Limited work to date has demonstrated the simulation of random fields over curved, non-rectangular domains. In many of these examples the models have simple geometries such as cylinders, in which the dependence upon the geometry may readily be prescribed explicitly through the choice of coordinate system, correlation function, and boundary conditions. For example, random fields were used to model geometric imperfections in cylindrical shell structures in [13], and geometric and boundary imperfections in cylindrical shells with cut-outs in [14]. In both cases the geometry was accounted for by parametrising the covariance function with respect to the circumferential direction using polar coordinates, and by imposing periodic boundary conditions. Monte Carlo Simulation of finite element models composed of triangular shells was undertaken in [15], with uncertainty in modulus, Poisson's ratio and thickness defined using the spectral representation method. Example applications were presented based upon a curved roof idealised as a cylindrical panel, and a hyperboloid geometry, however, the dependence of the correlation function upon the domain geometry was not explicitly discussed. The same method was extended to include geometric imperfections in [16], and applied to both a cylindrical panel and an axially compressed cylinder. In the latter example, a separable correlation structure was prescribed with respect to axial and circumferential directions, thereby explicitly accounting for the geometry. More recent effort towards experimental measurement, and stochastic simulation of geometric imperfections in cylindrical shells may be found in [17–19].

The simulation of random fields over complex domains is also often achieved through discretisation of the domain using the finite element mesh, and approximating the Karhunen–Loève eigenfunctions as a weighted sum of local basis functions defined on element domains. Such an approach enables these complex nonlinear functions to be approximated using low order, piecewise-continuous functions [10]. A commonly used approach is a Galerkin projection onto a basis defined by the finite element shape functions, which was first proposed in [1], and demonstrated upon a flat domain with curved boundary. Practical implications of using this projection technique in conjunction with commercial finite element codes were discussed in [20], and the resulting formulation applied to three demonstrative problems including a flat rectangular plate, flat plate with holes, and flat idealisation of an aircraft wing. An alternative finite element KLE method was proposed in [21], in which Lagrange polynomials were chosen to form the local basis, thus enabling the field to be evaluated at the Gauss integration points of each element, in order to non-intrusively integrate the variability into commercial finite element software ABAQUS. This approach was demonstrated upon flat domains representing a quarter-circle tube wall, and a retaining wall structure. A similar method using Lagrange

polynomials to interpolate random fields within finite elements was proposed in [22], and applied to example domains such as a quarter-circular tube and corrugated panel.

Another noteworthy class of methods used to simulate random fields over complex domains is based upon the principle of generating an initial set of samples over a simpler bounding domain, and discarding realisations in unwanted regions. Such an approach can in some cases circumvent the need to sample over complex domains. A 'finite cell' method was proposed in [10], and applied to a square domain with a circular cut-out. In this example, the limits of the Fredholm integral solved in the Karhunen–Loève Expansion are taken on the square bounding domain, and the integrand is assumed to be discontinuous at the boundaries of the physical domain defined at the cut-out. A 'domain independence' property was theorised in [23], which implied that the realisations of a random field approximated using KLE are independent of the domain geometry. This property relies upon the assumption that one of the domains in question is a subset of the second, and that the covariance function is unmodified under the change of domain. This property was exploited in order to model random fields on geometries defined as cut-outs from larger bounding domains. Demonstration problems included a square plate with circular cut-out and angle bracket with multiple cut-outs. A similar approach was presented in [24], in which Legendre polynomials were used to approximate random fields on the bounding domain.

Recently, an information-theoretic method for simulating elasticity tensors as random fields was proposed in [25], and demonstrated upon spherical and cylindrical domains in $\mathbb{R}^3$. In this approach, direction-dependent correlation length like parameters are prescribed via a diffusion field, and random field sample realisations are generated through solution of the resulting stochastic differential equation using the Galerkin method with a finite element basis. For the example geometries, it was possible to target specified spectral density functions using the correct choice of coordinate system and bounds. A similar sampling method was applied to the simulation of nonlinear strain energy functions as non-Gaussian random fields over complex domains in [26]. This approach was demonstrated upon a complex artery wall geometry, using a local coordinate system which varies spatially within the structure to follow the axial, circumferential, and through-thickness directions. This method relies upon targeting a covariance function through numerical experiments, rather than an explicit a priori definition. In [27], a diffusion maps metric was used to parametrise the covariance function of Gaussian processes, in order to account for intrinsic correlation structures occurring in large time-dependent datasets, which are insufficiently captured using a Euclidean metric. Also of note is the investigation in [28], in which it was found that the mathematical structure of a random field can be significantly altered through large geometrical transformations of the spatial domain, such as those induced during manufacturing processes.

Despite significant progress on the topic, there has been a relatively low uptake in the application of the stochastic finite element method to real-world engineering problems in the decades since its advent. Although many sophisticated methods have been developed for the simulation of random fields, these methods have typically only been demonstrated upon simple example geometries such as cylinders or spheres, or flat plates with non-rectangular boundaries wherein correlation functions may readily be defined using standard metrics such as the Euclidean distance. To the knowledge of the authors, there is no existing work in which the dependence of the correlation function upon the geometry of an arbitrary, curved, two-dimensional surface is discussed and defined explicitly. Furthermore, there is no existing guidance on how random fields parametrised using such a correlation function, may be simulated using commercial finite element software.

In this paper, an algorithm is proposed for simulating random fields defined over a general two-dimensional surface, discretised using a finite element mesh. The proposed algorithm is based upon parametrising the correlation function using the geodesic distance, which is estimated by solving the 'discrete geodesic problem' [29]. The correlation function is evaluated at the nodes of the model, and as such, this approach can be considered an extension of the point discretisation methods. The main contribution of the present work is to address two challenges associated with the practical application of random field methods to industrial finite element models:

- Explicit definition of a correlation function defined over an arbitrary curved geometry.
- Non-intrusive simulation of random fields using commercial, 'off the shelf' finite element software.

This paper is intended to serve as a simple guide for simulating random fields in existing industrial models, and as such, it is assumed throughout that the user is unable to modify the finite element mesh, and does not have access to the finite element shape functions. In order to demonstrate the potential impact, the proposed method is applied in

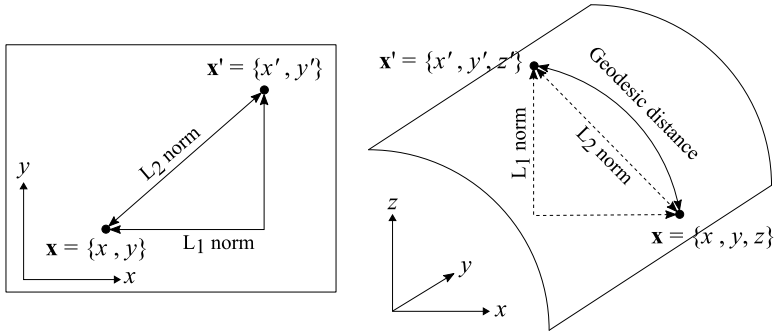

(a) Flat rectangular domain (b) Curved domain

Fig. 1. Distance norms on flat and curved spatial domains.

an uncertainty quantification case study on an industrial composite aircraft wing model, using commercial software package MSC Nastran.

The paper is structured as follows. In Section 2, the concept of a random field is introduced, and in Section 3 the proposed method for simulating random fields on curved meshes is presented. The method is demonstrated upon three example geometries in Section 4. Finally, the aircraft wing case study is presented in Section 5.

2. Random fields background

A random field, $H(\boldsymbol{x}, \theta)$, is defined as a collection of random variables indexed by spatial parameter $\boldsymbol{x} \in \Omega$, where Ω defines the geometry of the spatial domain, and $\theta \in \Theta$ is an outcome taken from sample space Θ. At a given spatial coordinate, $H(\boldsymbol{x}_0, \theta)$ is a random variable which defines the spread in H at $\boldsymbol{x}_0$. For a given outcome, $H(\boldsymbol{x}, \theta_0)$ defines a realisation of the field, which is a deterministic function in $\boldsymbol{x}$. A Gaussian random field may be defined entirely by its mean function, $\mu(\boldsymbol{x}) = \mathrm{E}[H(\boldsymbol{x}, \theta)]$, variance $\sigma^2(\boldsymbol{x}) = \mathrm{E}[(H(\boldsymbol{x}, \theta) - \mu(\boldsymbol{x}))^2]$, and autocorrelation function $\rho(\boldsymbol{x}, \boldsymbol{x}') = \mathrm{E}[(H(\boldsymbol{x}, \theta) - \mu(\boldsymbol{x}))(H(\boldsymbol{x}', \theta) - \mu(\boldsymbol{x}'))]/\sigma(\boldsymbol{x})\sigma(\boldsymbol{x}')$. The field is homogeneous if the mean and variance are constant, and the autocorrelation is parametrised completely by the difference $\boldsymbol{x} - \boldsymbol{x}'$ [2]. A commonly used correlation function may be defined as the exponential form

$$\rho(\boldsymbol{x}, \boldsymbol{x}') = \exp(-\|\boldsymbol{x} - \boldsymbol{x}'\|/c) \tag{1}$$

where $\| \bullet \|$ denotes a distance norm, and c is the correlation length. Parametrising the correlation function using the distance yields the physical intuition that the field is strongly correlated for nearby points at which it is likely to take similar values, and weakly correlated at points which are far apart, for which it is likely the field will differ. The correlation length dictates the typical length-scale across which variations occur. For a flat rectangular domain such as that shown in Fig. 1a, with $\boldsymbol{x} = \{x, y\}$, two possible exponential correlation functions may be defined as

$$\rho(\boldsymbol{x}, \boldsymbol{x}') = \exp(-|x - x'|/c_x)\exp(-|y - y'|/c_y) \tag{2}$$

$$\rho(\boldsymbol{x}, \boldsymbol{x}') = \exp(-\sqrt{(x - x')^2 + (y - y')^2}/c) \tag{3}$$

The L_1 norm used in Eq. (2), also known as the 'taxicab' norm, is often used for mathematical convenience as it enables a two-dimensional correlation function to be separated into the product of two one-dimensional functions. The L_2 norm used in Eq. (3), also known as the Euclidean norm, may be a more realistic measure of the physical correlation between points. These norms are illustrated in Fig. 1a.

While the distance norms used in Eqs. (2)–(3) may be used to define the correlation between points on a flat domain, they cannot give an accurate measure of this correlation over a curved surface such as that shown in Fig. 1b. The geodesic distance, defined as the arc-length of the shortest path between points $\boldsymbol{x}$ and $\boldsymbol{x}'$, is a reasonable alternative measure which may be used in the exponent of Eq. (1). While closed-form expressions for this distance exist for simple geometries, it is necessary to use numerical algorithms to determine this distance for a general surface. Such an algorithm is introduced in the subsequent section.

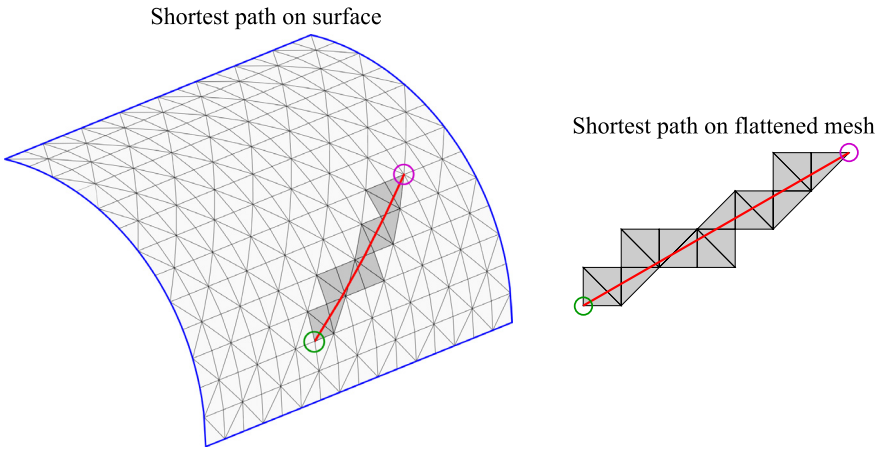

Fig. 2. Shortest path on a curved mesh, and equivalent straight path on a 'flattened' mesh.

3. Simulating random fields on curved domains

3.1. Overview

A method is now presented for simulating random fields across curved spatial domains. The algorithm is non-intrusive, and may be applied as a black box in order to generate samples across any two-dimensional surface, provided that this surface is discretised using a triangulated mesh. The approach is therefore a useful tool for uncertainty quantification using pre-defined finite element models in commercial, 'off the shelf' software. The geodesic algorithm used to define the covariance is introduced in Section 3.2, and point discretisation simulation approach is described in Section 3.3, before a summary is presented in Section 3.4.

3.2. The discrete geodesic problem

As discussed previously, the correlation function of a random field is often parametrised using the distance between points. On a curved surface, the shortest distance between points is known as the geodesic distance, and is illustrated in Fig. 1b. In this section, a class of algorithms for determining the shortest path between points on a finite element mesh is introduced. Such an algorithm was first proposed for non-convex geometries by Mitchell, Mount and Papadimitriou [29], which used a 'continuous Dijkstra's' algorithm to propagate shortest paths over a surface. In this paper, the implementation of [29] proposed in [30] is used. The implementation is not discussed in detail due to the black-box nature of its use, however, significant features are outlined in this section.

The fundamental concept exploited by the algorithm is that the shortest path between two points on an unfolded mesh is given by a straight line on an 'flattened' mesh, as illustrated in Fig. 2. The shortest path may change direction at 'saddle vertices' in non-convex geometries. Paths are propagated through the structure based upon an analogy with a ray of light emanating from the source node, in order to determine a window of possible paths through a sequence of edges, as illustrated in Fig. 3. The resulting windows behave as the nodes in Dijkstra's algorithm [31] for determining shortest paths on a graph, with the exception that the distance from the source to a particular edge interval is defined using a function rather than a unique value. Once the paths have been propagated through the mesh, the shortest path from source to destination node is retrieved as a sequence of edges, from which the geodesic distance is determined using the Euclidean metric on the flattened mesh.

In order to demonstrate performance of the algorithm in determining shortest paths around non-convex features, two examples are shown in Fig. 4 corresponding to a plate with circular hole, and a plate with curved boundaries. In both cases the algorithm determines a path around the circumference of the domain boundary, rather than cutting across the regions in which the domain is undefined. The proposed method therefore accurately models the effects of such features upon the field covariance.

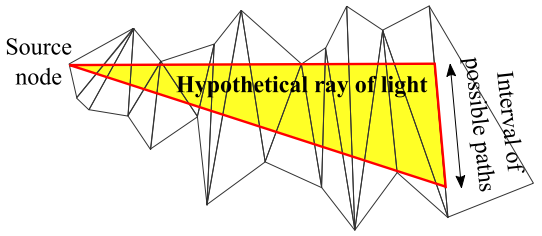

Fig. 3. Propagation of paths from source over a sequence of edges in a 'flattened' mesh, reproduced from [29].

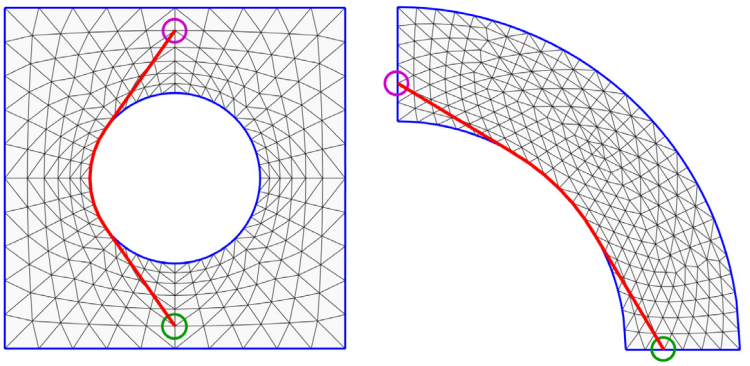

Fig. 4. Two examples of shortest paths across non-convex domains.

3.3. Simulation using point discretisation methods

In practical applications, random fields must be discretised such that they may be sampled as finite-dimension random variables. In point discretisation methods [2], the random field is evaluated at a discrete number of points in the spatial domain as a correlated random variable. For example, a homogeneous random field may be modelled at N nodes of a finite element model using a N-variate Gaussian random vector $\hat{\mathbf{H}}(\theta)$, which is distributed as

$$(\hat{\mathbf{H}}(\theta) - \mu)/\sigma \sim \mathcal{N}(0, \mathbf{R}) \tag{4}$$

where μ and σ are the mean and standard deviation, and $\mathbf{R}$ is an $N \times N$ correlation matrix with components

$$R_{ij} = \rho(\boldsymbol{x}_i, \boldsymbol{x}_j) \tag{5}$$

where ρ is the autocorrelation function and $\boldsymbol{x}_i$ and $\boldsymbol{x}_j$ are the coordinates of the ith and jth nodes respectively.

A correlated Gaussian random variable may be simulated by exploiting an orthogonal decomposition of the covariance matrix based upon principal components. Let λ_i and $\boldsymbol{\varphi}_i$ be eigenvalues and eigenvectors of an $N \times N$ symmetric and positive semi-definite correlation matrix $\mathbf{R}$. The eigenvalues may be arranged into a diagonal matrix $\boldsymbol{\Lambda} = \text{diag}(\lambda_1, \lambda_2, \ldots, \lambda_N)$, and the eigenvectors arranged columnwise into matrix $\boldsymbol{\Phi} = \{\boldsymbol{\varphi}_1, \boldsymbol{\varphi}_2, \ldots, \boldsymbol{\varphi}_N\}$, in order to give rise to an orthogonal decomposition in the form

$$\mathbf{R} = \boldsymbol{\Phi}\boldsymbol{\Lambda}\boldsymbol{\Phi}^T \tag{6}$$

Given this decomposition, the set of correlated Gaussian random variables may be simulated using the affine transformation

$$\hat{\mathbf{H}} = \mu + \sigma\boldsymbol{\Phi}\boldsymbol{\Lambda}^{1/2}\mathbf{u} \tag{7}$$

where $\mathbf{u}$ is a vector of N independent and identically distributed Gaussian random variables. It should be noted that this sampling procedure is reliant upon the assumption that the covariance matrix is positive semi-definite. In some cases of non-convex geometry, such as the examples shown in Fig. 4, covariance matrices were found to have small,

negative eigenvalues. In such cases the algorithm must be modified to retain only the positive eigenvalues and their corresponding eigenvectors, in which case Eq. (7) becomes

$$\hat{\mathbf{H}} = \mu + \sigma \boldsymbol{\Phi}_R \boldsymbol{\Lambda}_R^{1/2} \mathbf{u}_R \tag{8}$$

where $\boldsymbol{\Phi}_R = \{\boldsymbol{\varphi}_1, \boldsymbol{\varphi}_2, \ldots, \boldsymbol{\varphi}_{N_R}\}$, $\Lambda_R = \text{diag}(\lambda_1, \lambda_2, \ldots, \lambda_{N_R})$, $\mathbf{u}_R$ is an vector of N_R Gaussian-distributed variables, and N_R is the total number of positive eigenvalues.

It should be noted that the above approach is limited to simulating Gaussian random fields. If required, the method may readily be extended to simulating non-Gaussian fields as a translation process, defined using a nonlinear transformation of an underlying Gaussian random field of the form [32,33]

$$Z(\boldsymbol{x}, \omega) = g(Y(\boldsymbol{x}, \omega)) = F^{-1}[\Phi(Y(\boldsymbol{x}, \omega))] \tag{9}$$

where $Z(\boldsymbol{x}, \omega)$ is a non-Gaussian random field with marginal Cumulative Distribution Function (CDF), F, Φ denotes the standard Gaussian CDF, $Y(\boldsymbol{x}, \omega)$ is an underlying Gaussian field, and g denotes a nonlinear "memoryless" transformation. Care must taken to ensure that the correlation structure of transformed field matches the target correlation function. This matching is often undertaken through iteratively updating the correlation structure of the underlying Gaussian random field [32–35].

3.4. Simulation algorithm summary

In previous sections, individual components of the proposed method have been introduced. An overview of the complete approach is shown in Algorithm 1.

Algorithm 1 Curved-domain random field simulation approach

1: Use discrete geodesic algorithm to determine the length of the shortest path between each pair of nodes, $d(x_i, x_j) \ \forall \ i, j \in \{1, \ldots, N\}$.
2: Evaluate covariance matrix using geodesic distance between each pair of nodes, $R_{ij} = \exp(-d(x_i, x_j)/c)$.
3: Determine eigenvalues and eigenvectors of the covariance matrix, $\boldsymbol{\Lambda} = \text{diag}\,(\lambda_1, \lambda_2, \ldots, \lambda_N)$, $\boldsymbol{\Phi} = \{\boldsymbol{\varphi}_1, \boldsymbol{\varphi}_2, \ldots, \boldsymbol{\varphi}_N\}$.
4: Retain N_R positive eigenvalues and corresponding eigenvectors, $\boldsymbol{\Lambda}_R = \text{diag}\,(\lambda_1, \lambda_2, \ldots, \lambda_{N_R})$, $\boldsymbol{\Phi}_R = \{\boldsymbol{\varphi}_1, \boldsymbol{\varphi}_2, \ldots, \boldsymbol{\varphi}_{N_R}\}$.
5: Generate a set of N_R, independent and identically distributed Gaussian samples, $\mathbf{u} = \{u_1, u_2, \ldots, u_{N_R}\}, \quad u_i \sim \mathcal{N}(0, 1) \ \forall \ i$.
6: Project onto N-variate correlated Gaussian variable to give sample value at each node, $\mathbf{v} = \boldsymbol{\Phi}_R \boldsymbol{\Lambda}_R^{1/2} \mathbf{u}$.
7: Shift and scale sample properties in accordance with the required mean and standard deviation, $\hat{\mathbf{H}} = \sigma \mathbf{v} + \mu$.
8: Approximate element properties as average value of adjoining nodes.

The proposed method is advantageous in that it is relatively simple to implement, and relies entirely upon distinct black-box components. The method may be used in conjunction with commercially available finite element software, and there is no need to evaluate potentially expensive integrals, such as those required by the Galerkin method [1]. The discrete geodesic algorithm used in Step 1 is central to the approach. For a given mesh, this step needs only to be undertaken once, as the obtained data on geodesic distances may be re-used to generate samples for a variety of different correlation structures. The major limitation of the proposed method is that it may only be used to simulate stationary random fields, whose covariance is parametrised solely by the distance between points.

In Step 8, element properties are taken as an average of nodal values. It should be noted that this choice has been made for the sake of simplicity, and the algorithm may readily be modified to determine element properties using a variety of methods. The midpoint method [4] may be used, if in Step 1 distances are determined between element midpoints rather than the nodes, or variability may be explicitly integrated into stiffness matrices if the field is evaluated at the element Gauss points [5]. Sampled field values may also be interpolated within each element using the shape function method [6].

3.5. Computational cost

The primary aim of the present work is to address the parametrisation of the correlation function in surfaces of arbitrary geometry. For the sake of completeness, significant aspects of the computational cost of the proposed sampling method are discussed in this section, alongside suggestions for potential improvements. This discussion focuses upon the scaling of the required computation time with the number of nodes, as this can often be large in complex three-dimensional finite element models.

The computational efficiency of the presented method is limited by the algorithm used to evaluate the geodesic distance between all nodes in the mesh. In the original work by Mitchell, Mount and Papadimitriou (MMP) [29], the distance between a single source node and all destination nodes was achieved with a theoretical complexity $O(n^2 \log n)$. Chen and Han (CH) [36] later proposed an alternative algorithm with theoretical complexity $O(n^2)$, however, it was subsequently found to be outperformed by the MMP algorithm in practice [30]. In order to evaluate the covariance matrix, it is necessary to determine the distance between all nodes in the mesh. Assuming either the MMP or CH algorithms are applied sequentially using each node as a source, the required distances may be determined with complexity $O(n^3 \log n)$ and $O(n^3)$ respectively [37]. It should be emphasised that although this distance calculation is the most computationally expensive aspect of the method, this step need only be undertaken once for a given mesh, and data may be re-used in other simulations with different correlation structures. Recently, fast wavefront propagation [38], as well as a heat flow method [39], have been shown to achieve substantial reductions in the required computational expense compared with both MMP and CH algorithms.

The computation time required for the eigen-decomposition used in the proposed simulation of the random field is known to increase significantly with the matrix size, with complexity $O(n^3)$ when using Cholesky factorisation of symmetric, positive-definite matrices. Circulant embedding methods [40] were shown to achieve this eigen-decomposition with complexity $O(n \log n)$ by utilising the Fast Fourier Transform technique, however, this approach assumes that the field is simulated at regular grid points, and as such is not applicable to the complex geometries discussed in this paper. The generalised fast multi-pole method [41,42] was shown to solve the matrix eigenvalue problem resulting from finite element discretisation of Karhunen–Loève Expansions using a Krylov subspace eigensolver with a complexity $O(n \log n)$. To further reduce computation time, covariance matrices may be approximated using $\mathcal{H}$ matrices [43,44], a sparse hierarchical format wherein a matrix is partitioned into sub-blocks, with sub-blocks having low contribution to the system approximated using low-rank matrices. Such a technique has been shown to achieve the decomposition in approximately linear time [45].

It should be remarked that in practice, the mesh density required for structural calculations is unlikely to be identical to that required to accurately discretise the random field. The approach outlined in Algorithm 1 assumes analysis is undertaken for an existing model, and only a structural mesh exists. In such a situation, simulating the random field using the structural mesh is a pragmatic solution which enables analysis to be undertaken at all. In an ideal application, a separate mesh would be used to simulate the random field, with an appropriate density based upon the correlation length of the field. In such a case it would be possible to simulate random fields with high correlation lengths using relatively few nodes, thereby creating an additional means to reduce the computation time [46,3,21]. A convergence study may be undertaken using an appropriate error measure in order to identify a suitable mesh density. Error measures are typically defined [2,10] as spatial integrals and statistical moments of the point-wise approximation error, $\epsilon_H(\boldsymbol{x}, \theta) = H(\boldsymbol{x}, \theta) - \hat{H}(\boldsymbol{x}, \theta)$, given by the difference between the exact random field value, H, and its discretisation, $\hat{H}$. One such measure is the error variance, defined as [2,10]

$$\epsilon_\sigma(\boldsymbol{x}) = \mathrm{Var}[H(\boldsymbol{x}, \theta) - \hat{H}(\boldsymbol{x}, \theta)]/\mathrm{Var}[H(\boldsymbol{x}, \theta)] \tag{10}$$

Such error measures are difficult to calculate in general, as it is difficult to evaluate exact point-wise random field value H over complex surfaces without discretising the geometry to some extent. By assuming the random field is stationary and homogeneous, and exploiting the independence of random variables u_i from Algorithm 1, Eq. (10) may be expressed as

$$\epsilon_\sigma(\boldsymbol{x}) \approx 1 - \sum_{i=1}^{N} \phi_i(\boldsymbol{x})^2 \lambda_i \tag{11}$$

Noting that $\phi_i(\boldsymbol{x})$ is the ith eigenvector of the correlation matrix, which is defined only at the nodes of the model, it may be seen that Eq. (11) is only exact at the nodes. Should a global error measure be required, it is typical to

Table 1
Number of nodes, elements, and random variables used in modelling random fields on example meshes.

Geometry	Nodes	Elements	Random variables
Support Bracket	905	4900	888
Torus	2450	1634	2450
Aircraft	8757	17510	7741

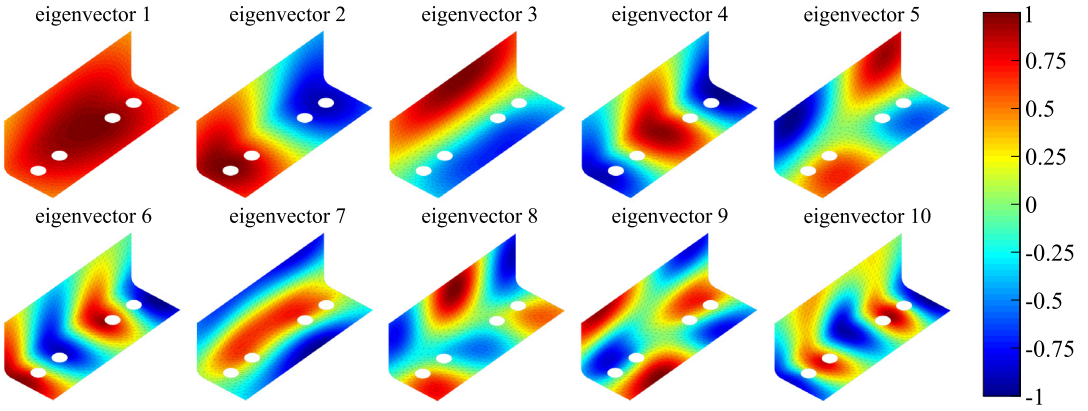

Fig. 5. Example eigenvectors for a support bracket.

integrate the error variance across the entire spatial domain [2,10], however, this may be difficult to evaluate in an arbitrary geometry. Using the proposed discretisation, an alternative measure may be the average of Eq. (11) taken across all nodes, or the maximum nodal variance error given by $\hat{\epsilon}_\sigma = \sup_{\boldsymbol{x}\in\Omega}|\epsilon_\sigma(\boldsymbol{x})|$.

4. Simulation on example domain geometries

In order to demonstrate the flexibility of the proposed method, the approach outlined in Algorithm 1 is applied to three example mesh geometries. The first example is a relatively simple support bracket geometry with multiple bolt holes. A torus is chosen as a second example, with more complicated geometry upon which shortest paths are more difficult to calculate analytically, as some of the geodesics are unbounded. Finally, an aircraft model is used to demonstrate application of the method to an arbitrary, complex geometry. The number of nodes and elements used in each example are detailed in Table 1.

It should be emphasised that these examples are chosen in order to demonstrate the flexibility of the algorithm for simulation over two-dimensional surfaces of arbitrary geometry, and do not necessarily represent realistic engineering problems. For example, an aircraft is a complex assembly of many components each of which is manufactured separately, and as such, in practice it would be necessary to model each of the components as independent random fields. An example of a more detailed analysis featuring multiple structural components is presented in Section 5.

It is important to note that the mesh geometry typically represents the manufactured configuration of a structure, which may not sufficiently describe the underlying random field. A simple example is the flat plate with hole shown in Fig. 4, which would likely be manufactured by cutting a hole from a flat plate, and as such, a Euclidean metric may better parametrise the underlying random field. The support bracket in Fig. 5 has been chosen as a more complex example which illustrates a similar situation. The Euclidean distance is clearly a poor metric with which to define correlation globally, as such a metric defines correlation across the effective hypotenuse between the horizontal and vertical faces. However, the Euclidean distance better describes the correlation in the locally flat region of the bolt holes. For a curved panel with circular cut-out, the Euclidean distance would not accurately describe the geometry of the panel prior to cutting, however, as this geometry is undefined in the mesh it is impossible to prescribe appropriate properties to the cut-out region. When modelling random fields over large structures with arbitrary geometry there may be hundreds of such features. The method proposed in Algorithm 1 is considered a pragmatic compromise which

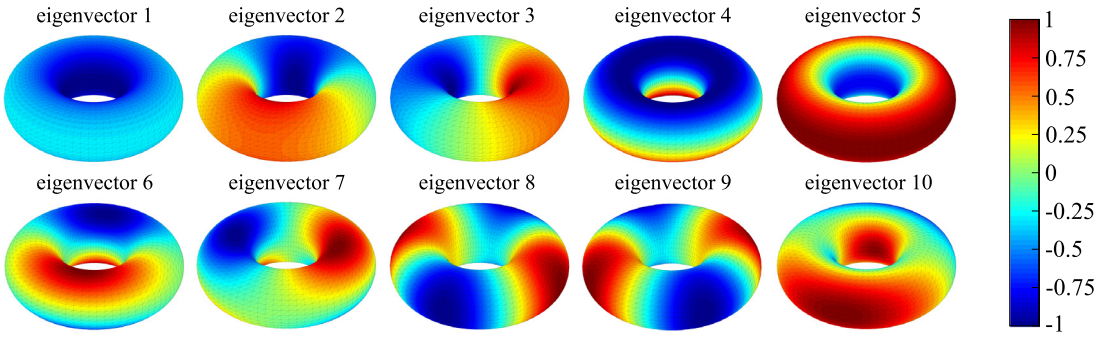

Fig. 6. Example eigenvectors for a torus.

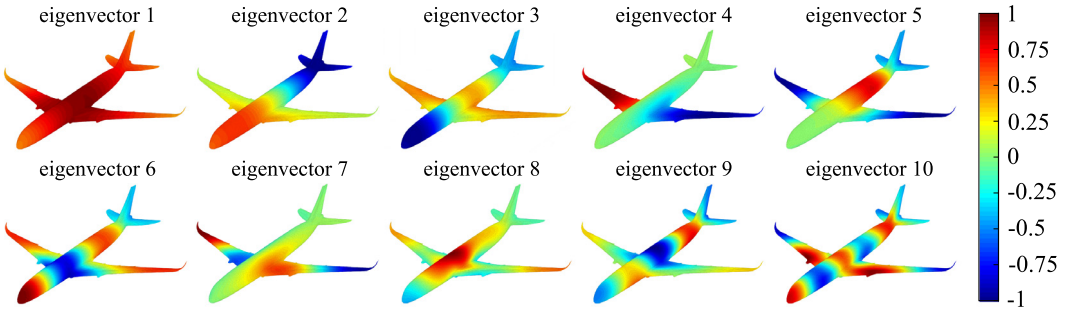

Fig. 7. Example eigenvectors for an aircraft model.

enables analysis to be undertaken, when such features are relatively small compared to global dimensions of the component.

In Algorithm 1, a random field is simulated as a random sum of eigenvectors of the correlation matrix, weighted by the corresponding eigenvectors. The first ten eigenvectors are shown for each of the example geometries in Figs. 5–7. Resulting random field sample realisations are shown in Fig. 8. In each case, the required number of random variables is based upon the number of positive eigenvalues of the $N_{\text{nodes}} \times N_{\text{nodes}}$ correlation matrix. The number of variables used to generate each of the example field samples is shown in Table 1.

5. Aircraft wing case study

5.1. Model definition

In this section, the simulation algorithm described above is applied in an uncertainty study for a composite aircraft wing. In order to demonstrate the potential impact of the proposed method, analysis is undertaken upon an industrial finite element model, using commercial finite element software package MSC Nastran.

Existing work modelling random fields in composite material properties has been limited to relatively simple geometries. For example, early work by Engelstad and Reddy [47] investigated the deflection of a spherical shell, and postbuckling of a flat plate using a point discretisation method. Karhunen–Loève Expansion was combined with a Rayleigh Ritz approach in [48], in order to model free vibration of composite cantilever plates with uncertain modulus and density. An intrusive formulation for the stochastic finite element stiffness matrices of flat composite laminates with uncertain out-of-plane stiffness was obtained in [49], and subsequently used in a stress analysis. A stochastic finite element method for non-Gaussian random fields based upon Optimal Linear Expansion was presented in [50]. Additionally, a non-intrusive approach was used in [51], in which KLE was combined with High-Dimensional Model Representations in the aeroelastic analysis of a composite rotor blade idealised as a beam. To the knowledge of the

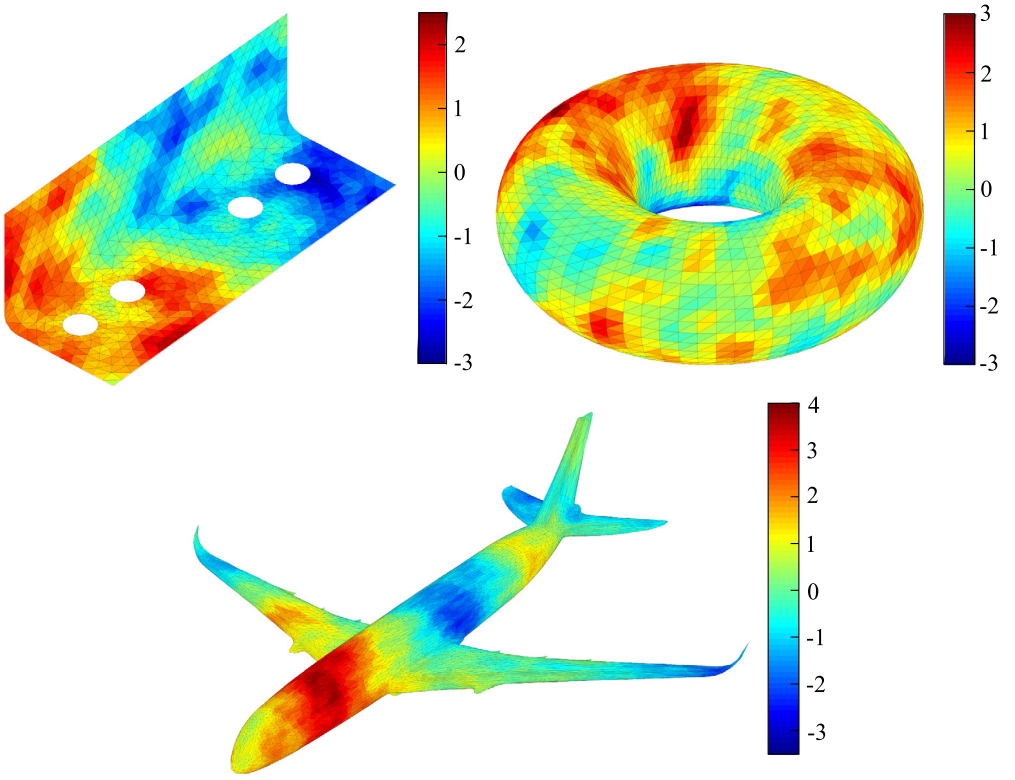

Fig. 8. Example sample realisations for example geometries.

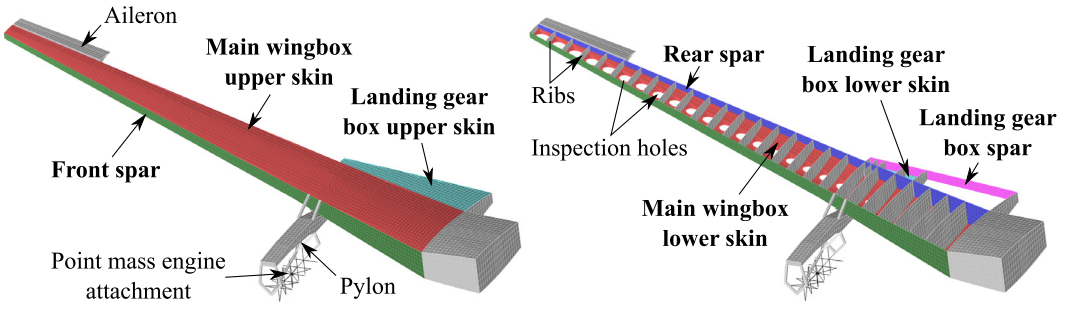

Fig. 9. Geometry and significant features of finite element wing model.

authors, the present study is the first application of a stochastic finite element framework to a composite wing model with realistic geometry.

An overview of the model geometry is shown in Fig. 9. The model consists of the skins and spars of a wingbox with attached landing gear box, including internal ribs and stringers (not pictured in Fig. 9). Also included are a flexible pylon with point mass engine attached using a cruciform of rigid elements, and a moveable aileron attached using spring elements. All parts of the wing are modelled as Carbon Fibre Reinforced Polymer (CFRP), with the exception of the pylon which is assumed to be made from aluminium. The skins, spars and rib covers are modelled using shell elements with specified lamina properties, whereas the stringers, spar caps and rib caps are modelled using beam elements with equivalent homogenised laminate properties. The layup of all composite parts are assumed to be quasi-isotropic.

In the present study, uncertainty is modelled in the longitudinal modulus (E_{11}), transverse modulus (E_{22}), shear modulus (G_{12}) and Poisson's ratio (ν_{12}) of the skins and spars of the main wingbox and landing gear box. Each of

Table 2
Mean and coefficient of variation of random fields [52,53].

	E_{11} (GPa)	E_{22} (GPa)	G_{12} (GPa)	ν_{12}
Mean	148.0	10.3	5.93	0.27
COV (%)	4	4.8	2.9	6

Table 3
Number of nodes, elements, and random variables required to model each random field.

Component	Nodes	Elements	Random variables
Main wingbox upper skin	4983	4748	4983
Main wingbox lower skin	6339	5648	5750
Front spar	2373	2028	2373
Rear spar	2373	2028	2373
Landing gear box upper skin	451	420	451
Landing gear box lower skin	145	124	145
Landing gear box spar	364	306	364

the parts modelled as a random field is highlighted in bold in Fig. 9. All random fields are assumed to be Gaussian distributed, with mean and coefficient of variation as defined in Table 2. These values are taken from the experimental studies outlined in [52], with the exception of the Poisson's ratio whose coefficient of variation is taken from [53]. In general, such properties are typically cross-correlated. Due to a lack of experimental data on the correlation between each property, it was conservatively assumed that each of the properties in Table 2 may be modelled as an independent random field. The use of Gaussian distributions to simulate elastic moduli is often criticised, as such distributions are unbounded. This choice of distribution was, however, considered acceptable in this application, as in practice the distribution parameters specified in Table 2 gave rise to negative elastic moduli with negligible probability. The correlation length is varied across a range of values in each case study. The random fields are sampled at the nodes of each element.

The algorithm proposed in this paper is required to model the random fields in this example application due to the curved upper and lower surfaces of the wing. The inspection holes in the lower skin are a non-convex feature which also affects the definition of the random field. Four random fields are modelled in the properties of seven components, resulting in a total of twenty eight random fields. The total number of variables required to represent each random field corresponds to the number of positive eigenvalues of the $N_{\text{nodes}} \times N_{\text{nodes}}$ covariance matrix. Example numbers of variables required to model each component are summarised in Table 3 for a correlation length equal to a third of the wing semi-span. In this example the 28 random fields may be modelled using a total of 460292 random variables. As previously discussed, it may be possible to reduce the required computation time and number of random variables by using a coarse mesh to sample the field in the higher correlation length examples, however, such an analysis is beyond the scope of the present work.

Due to the extremely large number of variables, it is only feasible to use Monte Carlo Simulation for uncertainty propagation. In the subsequent sections, uncertainty quantification case studies are presented for vibration and buckling of the wing. In both case studies, results are based upon simulation of 2500 sample realisations. An example realisation of one input random field sample is shown in Fig. 10.

5.2. *Free vibration analysis*

In this section, results are presented for free vibration of the wing. Normal modes analysis is undertaken using SOL 103 in MSC Nastran. Initially, random fields are assumed to have a correlation length equal to a third of the wing semi-span. Probability Density Functions (PDFs) for the natural frequency of the first 5 modes are shown in Fig. 11. In order to display trends over the broader number of modes considered in the analysis, the mean and standard deviation of the natural frequency of the first 20 modes are shown in Fig. 12. In both figures the frequencies have been normalised using the nominal, deterministic frequency of the first mode.

The Modal Assurance Criterion (MAC) has been used to investigate variations in the mode shapes under the input uncertainty. In order to determine statistics for the MAC, each mode shape, of each Monte Carlo sample, is compared

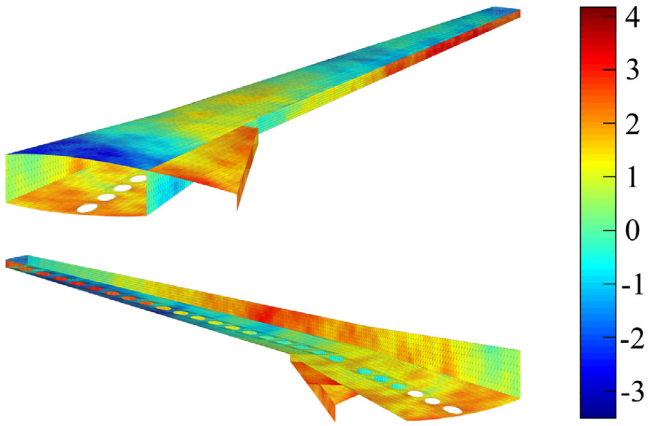

Fig. 10. Example standard Gaussian random field sample defined over wing surface.

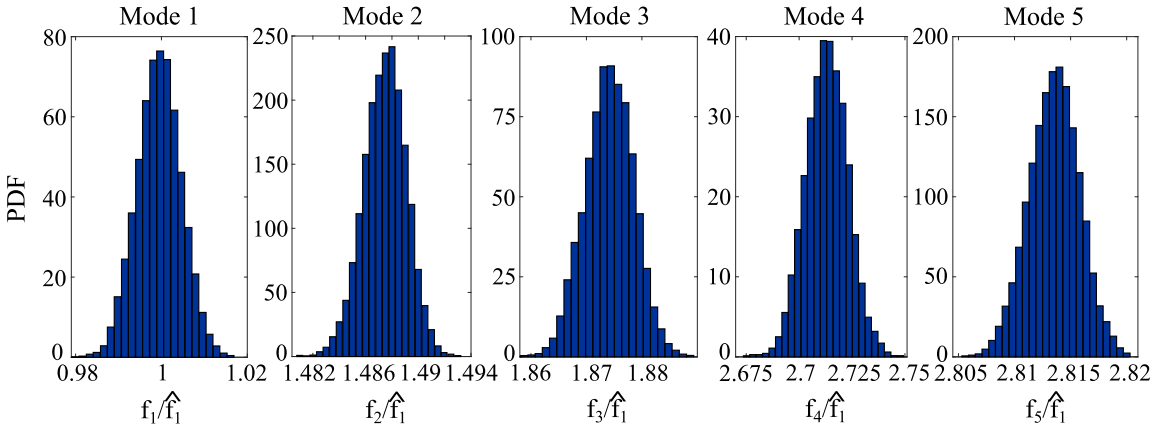

Fig. 11. Probability Density Functions of normalised natural frequency of first five modes.

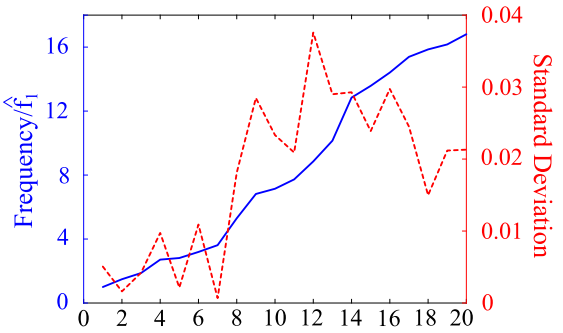

Fig. 12. Mean and standard deviation of normalised natural frequency of first 25 modes.

with each mode shape of a reference sample using

$$\mathrm{MAC}_{j,k}^{(i)} = \frac{|\boldsymbol{\phi}_{i,j}^{\mathrm{T}}\boldsymbol{\phi}_{\mathrm{ref},k}|^2}{(\boldsymbol{\phi}_{i,j}^{\mathrm{T}}\boldsymbol{\phi}_{i,j})(\boldsymbol{\phi}_{\mathrm{ref},k}^{\mathrm{T}}\boldsymbol{\phi}_{\mathrm{ref},k})} \tag{12}$$

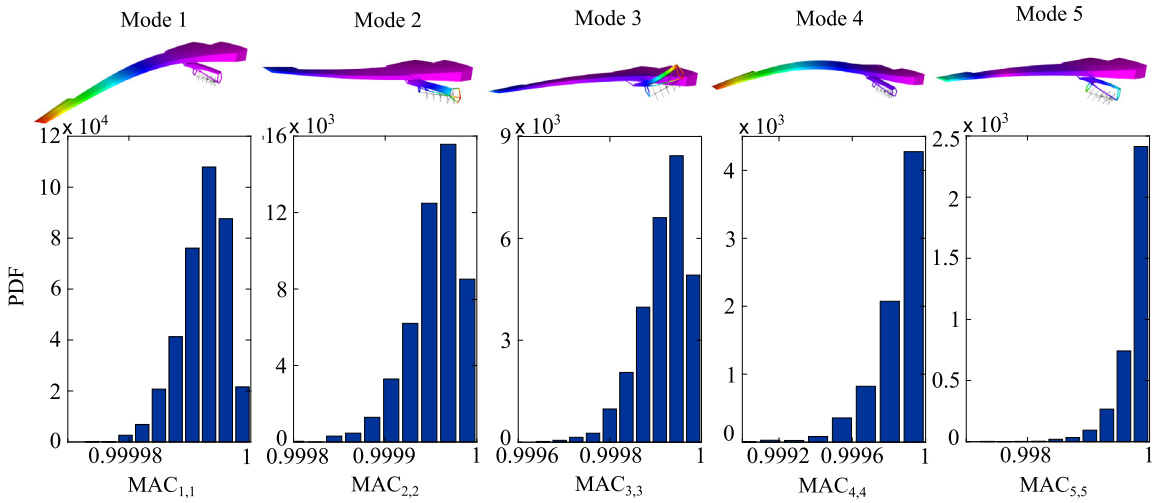

Fig. 13. Probability Density Functions for MAC of the first 5 vibration modes.

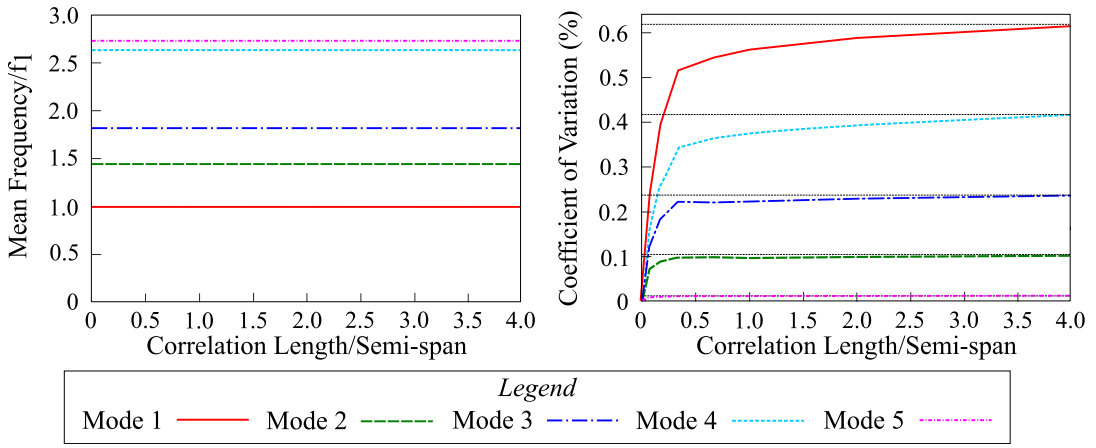

Fig. 14. Mean and coefficient of variation of normalised natural frequency with varying correlation length.

where $\mathrm{MAC}^{(i)}_{j,k}$ is the ith sample of the jth row and kth column of the MAC, $\boldsymbol{\phi}_{i,j}$ is the jth eigenvector of the ith output sample, and $\boldsymbol{\phi}_{\mathrm{ref},k}$ is the kth eigenvector of the reference sample. The reference eigenvectors are taken from an analysis using the mean values of the input random fields. PDFs for the first 5 diagonal entries of the MAC are shown in Fig. 13, alongside with illustrations of the reference mode-shapes. These plots show the extent to which mode-shapes vary from the reference sample, with a value of unity indicating identical mode-shapes, and zero indicating no similarity.

From Fig. 11 it can be seen that the natural frequencies of the first 5 modes approximately follow a Gaussian distribution, and as such, it is sufficient to understand trends using the mean and standard deviation plots in Fig. 12. The mean increases in an approximately linear trend with mode number, however, there is no such clear underlying trend in the standard deviation. Typically, the higher standard deviations correspond to modes dominated by span-wise bending, whereas lower standard deviations correspond to modes dominated by swaying of the pylon, in which uncertainty is not modelled. There is very little variation in the mode shapes evident in Fig. 13, in which the MAC varies in the range [0.999 1]. This insignificant level of variability can likely be attributed to the global nature of the mode shapes, which are insensitive to localised variations in material properties.

A parametric study has been undertaken in order to investigate the effects of varying the correlation length, by repeating the above analysis across a range of different values. The correlation length is varied from zero, in which

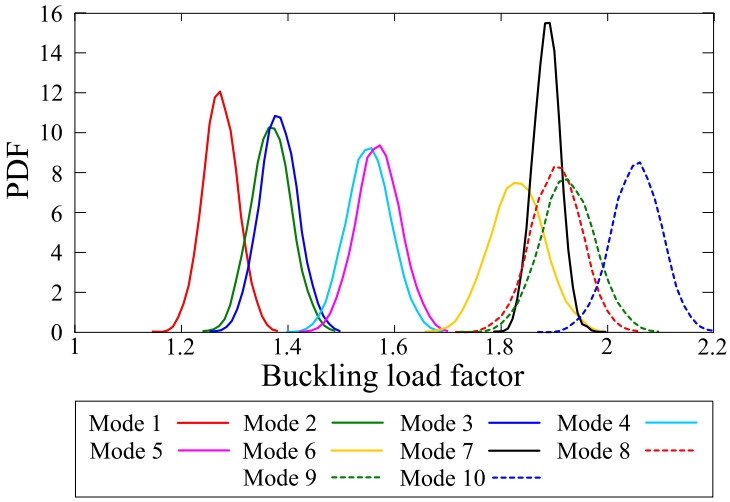

Fig. 15. Probability Density Functions of buckling load factor of first ten modes.

the properties of each finite element are assumed to vary independently of one another, to infinity, in which all of the elements for a particular part are assumed to be homogeneous. Resulting trends in the mean and coefficient of variation of the normalised natural frequency of the first 5 modes are shown in Fig. 14.

The mean of each natural frequency is insensitive to the value of the correlation length used in the analysis. The coefficient of variation increases with correlation length up to an upper bound defined for an infinite correlation length, represented as a dotted black line in Fig. 14. This upper bound corresponds to homogeneous properties across all elements in a given random field sample. As the correlation length decreases towards zero, whereby all elements have independently distributed values, the standard deviation decreases significantly. In this case the uncertainty averages out across the entire spatial domain for random fields with shorter correlation lengths. In this instance, it is therefore conservative to model each component using homogenised properties.

5.3. Buckling analysis

In this section, results are presented for buckling analysis of the wing undertaken using SOL 105 in MSC Nastran. Loads on the wing are determined in a static aeroelastic analysis for a 2.5 g pull-up manoeuvre, with aerodynamics modelled using the doublet lattice panel method. A considerable amount of mode-switching was noted across the set of raw data output from Nastran. As such, in post-processing it was necessary to sort the buckling load. This sorting was achieved by grouping together results with the most similar mode-shapes, determined using the MAC as defined in Eq. (12). The underlying principle is that of allocating results to a mode such that those with the highest MAC value are given priority, thereby first allocating data to modes for which there is a greater degree of confidence.

Probability Density Functions for the sorted buckling loads are shown for the first 10 modes in Fig. 15, and the mean and standard deviation are shown in Fig. 16. Additionally, PDFs for the diagonal entries of the MAC of the sorted eigenvectors are shown for the first 5 modes in Fig. 17, alongside images of the reference mode shapes. As in the previous example, trends in the mean and standard deviation of the buckling load across a range of correlation lengths are shown in Fig. 18.

It can be seen that the PDFs of the individual buckling loads are approximately Gaussian distributed. There is considerable cross-over of the PDFs associated with the higher modes, which could explain some of the mode-switching noted in the unsorted output data. In modes 1–6 the mean and standard deviation of the buckling load increase with parallel trends, however, mode 7 has a considerably lower standard deviation which may be attributed to the fact that the mode in question involves components in which uncertainty has been neglected. Modes 8–10 have comparable standard deviations.

The PDFs in Fig. 17 show considerable levels of variability in the mode shapes. These changes in the MAC are continuous, and indicate that the mode shapes vary gradually with variations in properties, rather than undergoing a

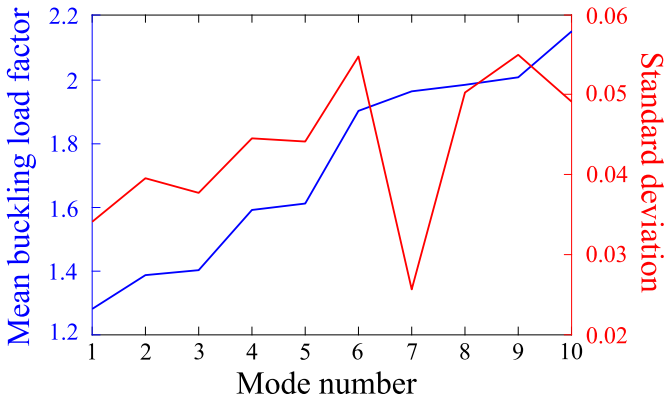

Fig. 16. Mean and standard deviation of buckling load factor of first ten modes.

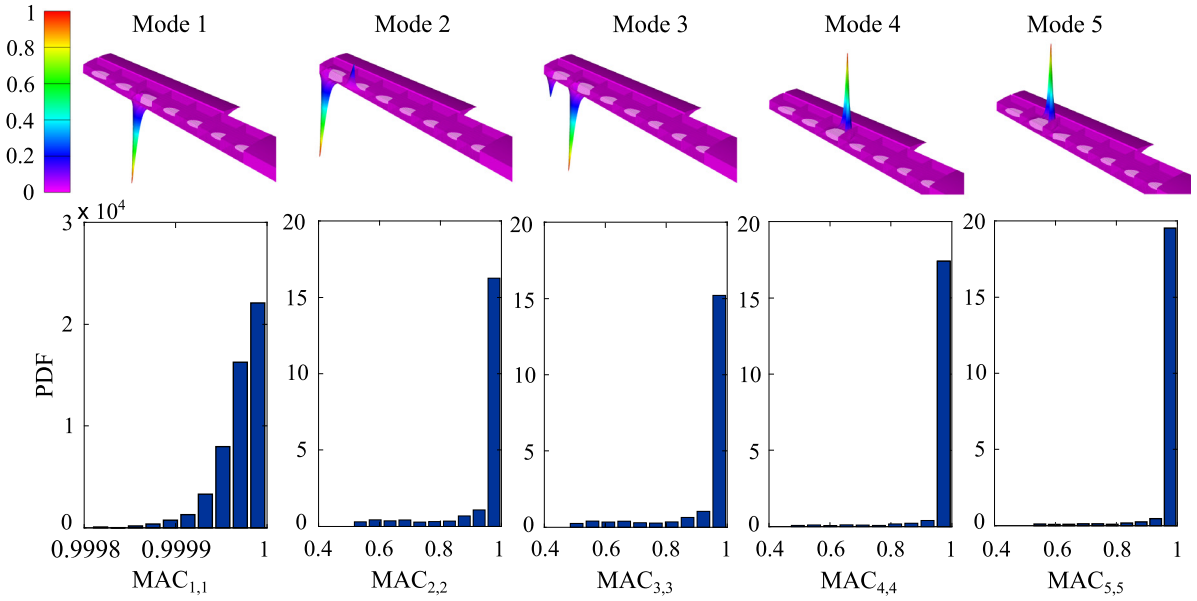

Fig. 17. Probability Density Functions for MAC of the first 5 buckling modes.

discrete mode switch. The variations in MAC for modes 2–5 are much larger than those in the vibration case study, typically taking values in the range [0.4, 1]. Given that the modes in question relate to localised buckling of panels between ribs, it is intuitive that the deflected shape should be more sensitive to localised variations in properties, compared with the vibration modes in Fig. 13 which concern deformation of entire wing. This phenomenon could also give rise to the mode-switching noted in the raw data.

Finally, a similar trend may be noted from the correlation length investigation as in the vibration case study, in that the standard deviation decreases as the correlation length tends towards zero. This result implies that although the localised variations in stiffness can give rise to considerable variability in the mode shapes, for smaller correlation lengths there is an averaging effect across the panels which leads to a reduced level of variability in the buckling load itself.

6. Conclusions

A method has been presented for simulating stationary random fields over curved two-dimensional surfaces. This method has been developed in order to address the fundamental issue of defining the correlation function on such

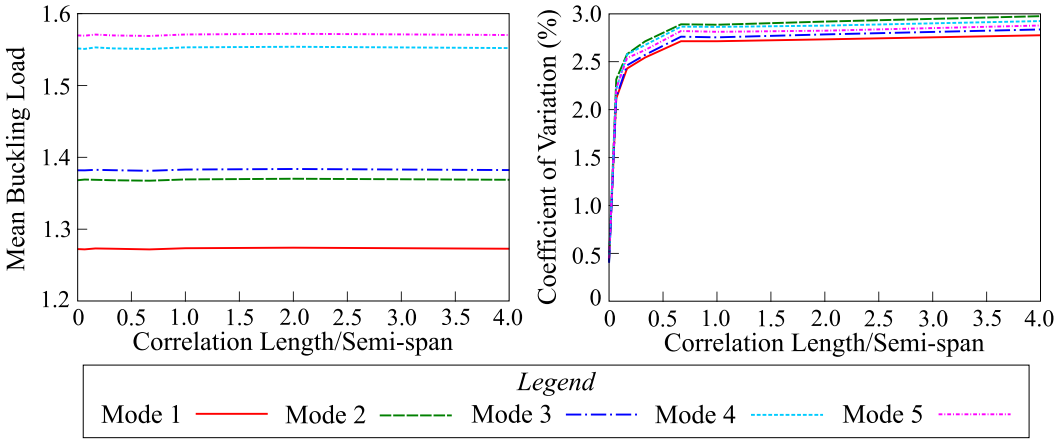

Fig. 18. Mean and coefficient of variation of buckling load of the first five modes, with varying correlation length.

surfaces, and its subsequent evaluation in practical applications, as the dependence of this correlation function upon complex geometries is not trivial to accommodate in practice. A focus was placed upon non-intrusive simulation of the resulting random field in realistic finite element models, using third party software, in order to facilitate future usage in industrial applications. Major contributions of this method may be summarised as:

- Parametrisation of the correlation function using the geodesic distance, in order to account for dependence upon model geometry.
- Practical guidance on evaluating the proposed correlation function on a general meshed surface of arbitrary geometry through solution of the 'discrete geodesic problem.'
- Definition of a simple methodology for non-intrusive simulation of the resulting random field using 'off the shelf', commercial finite element software, based upon point-discretisation methods.
- Demonstration of potential impact of method through application in an uncertainty quantification case study for an industrial finite element model of a composite aircraft wing with uncertain material properties.

The above work therefore addresses theoretical aspects of the domain dependence of the correlation function, develops a methodology for implementing the theory in practice, and demonstrates this methodology in application to a real-world industrial problem. This method requires only a one-off application of a black-box algorithm for a given mesh, does not require the evaluation of expensive multi-dimensional integrals, or access to finite-element shape functions. The proposed method has been designed to be easy to apply to any finite element shell model, using any software. This approach will therefore be beneficial for future use as a simple tool for simulating random fields in pre-existing, industrial finite element models.

Acknowledgement

The authors acknowledge the financial support received from Engineering Research Network Wales (Sêr Cymru National Research Networks) with Grant No. NRN 102.

References

[1] R.G. Ghanem, P.D. Spanos, Stochastic Finite Elements: A Spectral Approach, Springer-Verlag, New York, 1991.
[2] B. Sudret, A. Der-Kiureghian, Stochastic Finite Element Methods and Reliability: State-Of-The-Art Report. Technical Report UCB/SEMM-2000/08, Department of Civil & Environmental Engineering, University of California, Berkeley, 2000.
[3] G. Stefanou, The stochastic finite element method: Past, present and future, Comput. Methods Appl. Mech. Engrg. 198 (9) (2009) 1031–1051.
[4] A. Der Kiureghian, J. Ke, The stochastic finite element method in structural reliability, Probab. Eng. Mech. 3 (2) (1988) 83–91.
[5] H.G. Matthies, C.E. Brenner, C.G. Bucher, C.G. Soares, Uncertainties in probabilistic numerical analysis of structures and solids-Stochastic finite elements, Struct. Saf. 19 (3) (1997) 283–336.
[6] W.K. Liu, T. Belytschko, A. Mani, Random field finite elements, Internat. J. Numer. Methods Engrg. 23 (1986) 1831–1845.

[7] C. Li, A. Der Kiureghian, Optimal discretization of random fields, J. Eng. Mech. 119 (6) (1993) 1136–1154.
[8] E. Vanmarcke, M. Grigoriu, Stochastic finite element analysis of simple beams, J. Eng. Mech. 109 (5) (1983) 1203–1214.
[9] J. Zhang, B. Ellingwood, Orthogonal series expansions of random fields in reliability analysis, J. Eng. Mech. 120 (12) (1994) 2660–2677.
[10] W. Betz, I. Papaioannou, D. Straub, Numerical methods for the discretization of random fields by means of the Karhunen-Loève expansion, Comput. Methods Appl. Mech. Engrg. 271 (Supplement C) (2014) 109–129.
[11] M. Shinozuka, G. Deodatis, Simulation of stochastic processes by spectral representation, Appl. Mech. Rev. 44 (4) (1991) 191–204.
[12] M. Shinozuka, G. Deodatis, Simulation of multi-dimensional gaussian stochastic fields by spectral representation, Appl. Mech. Rev. 49 (1) (1996) 29–53.
[13] C.A. Schenk, G.I. Schuëller, Buckling analysis of cylindrical shells with random geometric imperfections, Int. J. Non-Linear Mech. 38 (7) (2003) 1119–1132.
[14] C.A. Schenk, G.I. Schuëller, Buckling analysis of cylindrical shells with cutouts including random boundary and geometric imperfections, Comput. Methods Appl. Mech. Engrg. 196 (35) (2007) 3424–3434.
[15] G. Stefanou, M. Papadrakakis, Stochastic finite element analysis of shells with combined random material and geometric properties, Comput. Methods Appl. Mech. Engrg. 193 (1) (2004) 139–160.
[16] V. Papadopoulos, M. Papadrakakis, The effect of material and thickness variability on the buckling load of shells with random initial imperfections, Comput. Methods Appl. Mech. Engrg. 194 (12) (2005) 1405–1426.
[17] C. de Paor, K. Cronin, J.P. Gleeson, D. Kelliher, Statistical characterisation and modelling of random geometric imperfections in cylindrical shells, Thin-Walled Struct. 58 (2012) 9–17.
[18] I. Vryzidis, G. Stefanou, V. Papadopoulos, Stochastic stability analysis of steel tubes with random initial imperfections, Finite Elem. Anal. Des. 77 (2013) 31–39.
[19] J. Kepple, M. Herath, G. Pearce, G. Prusty, R. Thomson, R. Degenhardt, Improved stochastic methods for modelling imperfections for buckling analysis of composite cylindrical shells, Eng. Struct. 100 (2015) 385–398.
[20] S.K. Sachdeva, P.B. Nair, A.J. Keane, On using deterministic FEA software to solve problems in stochastic structural mechanics, Comput. Struct. 85 (5) (2007) 277–290.
[21] Shen Shang, Gun Jin Yun, Stochastic finite element with material uncertainties: Implementation in a general purpose simulation program, Finite Elem. Anal. Des. 64 (Supplement C) (2013) 65–78.
[22] A. Kundu, S. Adhikari, M.I. Friswell, Stochastic finite elements of discretely parameterized random systems on domains with boundary uncertainty, Internat. J. Numer. Methods Engrg. 100 (3) (2014) 183–221.
[23] S. Pranesh, D. Ghosh, Faster computation of the Karhunen-Loève expansion using its domain independence property, Comput. Methods Appl. Mech. Engrg. 285 (Supplement C) (2015) 125–145.
[24] Iason Papaioannou, Non-Intrusive Finite Element Reliability Analysis: Structural Reliability Analysis With “Black Box” Finite Element Programs, Springer-Verlag, 2013.
[25] B. Staber, J. Guilleminot, Stochastic modeling and generation of random fields of elasticity tensors: A unified information-theoretic approach, C. R. Méc. 345 (6) (2017) 399–416.
[26] B. Staber, J. Guilleminot, A random field model for anisotropic strain energy functions and its application for uncertainty quantification in vascular mechanics, Comput. Methods Appl. Mech. Engrg. 333 (2018) 94–113.
[27] C. Thimmisetty, A. Khodabakhshnejad, N. Jabbari, F. Aminzadeh, R. Ghanem, K. Rose, J. Bauer, C. Disenhof, Multiscale Stochastic Representation in High-Dimensional Data Using Gaussian Processes with Implicit Diffusion Metrics BT in: Proc. Dynamic Data-driven Environmental Systems Science Conference, Nov 5–7 2014, Massachusetts Institute of Technology, Cambridge, Massachusetts, USA, 2015, pp. 157–166.
[28] R. Ghanem, C. Soize, Remarks on stochastic properties of materials through finite deformations, Int. J. Multiscale Comput. Eng. 13 (4) (2015).
[29] J. Mitchell, D. Mount, C. Papadimitriou, The discrete geodesic problem, SIAM J. Comput. 16 (4) (1987) 647–668.
[30] V. Surazhsky, T. Surazhsky, D. Kirsanov, S.J. Gortler, H. Hoppe, Fast exact and approximate geodesics on meshes, ACM Trans. Graph. 24 (3) (2005) 553–560.
[31] E.W. Dijkstra, A note on two problems in connexion with graphs, Numer. Math. 1 (1) (1959) 269–271.
[32] F. Yamazaki, M. Shinozuka, Digital generation of NonGaussian stochastic fields, J. Eng. Mech. 114 (7) (1988) 1183–1197.
[33] M. Grigoriu, Simulation of stationary Non-Gaussian translation processes, J. Eng. Mech. 124 (2) (1998) 121–126.
[34] G. Deodatis, R.C. Micaletti, Simulation of highly skewed non-gaussian stochastic processes, J. Eng. Mech. 127 (12) (2001) 1284–1295.
[35] M.D. Shields, G. Deodatis, P. Bocchini, A simple and efficient methodology to approximate a general non-Gaussian stationary stochastic process by a translation process, Probab. Eng. Mech. 26 (4) (2011) 511–519.
[36] J. Chen, Y. Han, Shortest paths on a polyhedron, Int. J. Comput. Geom. Appl. 6 (2) (1996) 127–144.
[37] M. Balasubramanian, J.R. Polimeni, E.L. Schwartz, Exact geodesics and shortest paths on polyhedral surfaces, IEEE Trans. Pattern Anal. Mach. Intell. 31 (6) (2009) 1006–1016.
[38] C. Xu, T.Y. Wang, Y. Liu, L. Liu, Y. He, Fast wavefront propagation (FWP) for computing exact geodesic distances on meshes, IEEE Trans. Vis. Comput. Graphics 21 (7) (2015) 822–834.
[39] K. Crane, C. Weischedel, M. Wardetzky, Geodesics in heat: A new approach to computing distance based on heat flow, ACM Trans. Graph. 32 (5) (2013) 152:1—-152:11.
[40] C. Dietrich, G. Newsam, Fast and exact simulation of stationary gaussian processes through circulant embedding of the covariance matrix, SIAM J. Sci. Comput. 18 (4) (1997) 1088–1107.

[41] P. Frauenfelder, C. Schwab, R.A. Todor, Finite elements for elliptic problems with stochastic coefficients, Comput. Methods Appl. Mech. Engrg. 194 (2) (2005) 205–228.
[42] C. Schwab, R.A. Todor, Karhunen-Loève approximation of random fields by generalized fast multipole methods, J. Comput. Phys. 217 (1) (2006) 100–122.
[43] B.N. Khoromskij, A. Litvinenko, H.G. Matthies, Application of hierarchical matrices for computing the Karhunen-Loève expansion, Computing 84 (1) (2009) 49–67.
[44] D.L. Allaix, V.I. Carbone, Karhunen–Loève decomposition of random fields based on a hierarchical matrix approach, Internat. J. Numer. Methods Engrg. 94 (11) (2013) 1015–1036.
[45] M. Feischl, F.Y. Kuo, I.H. Sloan, Fast random field generation with H-matrices, Numer. Math. (2018).
[46] D.C. Charmpis, M. Papadrakakis, Improving the computational efficiency in finite element analysis of shells with uncertain properties, Comput. Methods Appl. Mech. Engrg. 194 (12) (2005) 1447–1478.
[47] S.P. Engelstad, J.N. Reddy, Probabilistic nonlinear finite element analysis of composite structures, AIAA J. 31 (2) (1993) 362–369.
[48] P. Venini, C. Mariani, Free vibration of uncertain composite plates via stochastic Rayleigh-Ritz approach, Comput. Struct. 64 (1) (1997) 407–423.
[49] M.F. Ngah, A. Young, Application of the spectral stochastic finite element method for performance prediction of composite structures, Compos. Struct. 78 (3) (2007) 447–456.
[50] P. Sasikumar, R. Suresh, S. Gupta, Analysis of CFRP laminated plates with spatially varying non-Gaussian inhomogeneities using SFEM, Compos. Struct. 112 (2014) 308–326.
[51] S. Murugan, R. Chowdhury, S. Adhikari, M.I. Friswell, Helicopter aeroelastic analysis with spatially uncertain rotor blade properties, Aerosp. Sci. Technol. 16 (1) (2012) 29–39.
[52] K. Marlett, Y. Ng, J. Tomblin, Hexcel 8552 IM7 prepreg 190 gsm & 35%RC qualification material property data report advanced materials performance. NCAMP test report: CAM-RP-2010-002 Rev A, National Institute for Aviation Research, Wichita State University, Kansas, USA, 2011.
[53] H.K. Jeong, R.A. Shenoi, Probabilistic strength analysis of rectangular FRP plates using Monte Carlo simulation, Comput. Struct. 76 (1–3) (2000) 219–235.